# Remaining Useful Life Prediction via Computation of Physical and Material Properties

Navid Zaman[1], Milo Cooper[2], and Frank M. Juarez[3]

[1,2] *PHM Technology, Melbourne, Victoria, 3068, Australia*
*navid.zaman@phmtechnology.com*

[3]*PHM Technology US Corp., San Antonio, Texas, USA*

## ABSTRACT

Remaining useful life (RUL) prediction is a crucial aspect of predictive maintenance, enabling industries to optimize asset longevity and minimize unexpected failures. RUL becomes increasingly difficult with system complexity. Such systems are built up of components exhibiting known material properties. When degradation occurs, these materials are predictably affected and can indicate the remaining life of the system, both directly and indirectly. Changes reflected from damage, ageing and wear are particularly detectable in stiffness of materials, for example. This paper aims to utilize the physics and domain knowledge of systems along with material degradation indicators such as Young's Modulus and the interdependencies between such metrics, to accomplish RUL with a deeper understanding of wear and fatigue as compared to purely data-driven methods. Experimental studies and computational simulations demonstrate the effectiveness of this approach, offering a novel perspective on predictive maintenance strategies.

## 1. INTRODUCTION

Most RUL strategies involve using run-to-failure historical data to generate and forecast a health index or degradation metric. While such a variable may be determined by a subject matter expert (SME), they generally tend to function as a trend of the system that indicates an anomaly (Wang, Zhao, & Addepalli, 2020). Most often, the degradation metric is a function of measured variables from the system or component but does not relate to the physics or dynamics of the machine(s). When deciding upon an index to determine degradation, there are more factors to consider rather than how well it assumes the remaining life of the asset and whether it is easy to forecast. The main aspects of a good degradation metric are:



- Be physically meaningful values.
- Calculatable from physical measurements.
- Time varying
- Inputs into the state space equation.
- Change in metric leads to change in measurable system behavior

To this end, a physics-based approach is favorable, since there is less in the way of presumption and predictions are more explainable. Strong candidates for such criteria are material degradation metrics – calculated from measured variables, they indicate wear clearly (all material experience some form of wear over time) and are closely linked to the system/component dynamics.

Such strategies have been devised for component-based RUL prediction – usually involving a hybrid method of combining data-driven techniques with domain knowledge (Beaulieu, Jha, Garnier & Cerbah, 2024) However, a system RUL will require better than simply aggregating or obtaining the minimum component RUL predictions since interdependencies between degradation metrics make this task much more complex.

## 2. MATERIAL DEGRADATION

All systems, components and parts are made up of materials with known properties. These materials experience stress and strain over the lifecycle of the asset. Most predictable failures occur because of fatigue and wear of critical parts. Hence, understanding of the material properties, particularly the Young's Modulus (measure of stress vs strain) of said parts and their relations to the system can be a reliable indicator of system RUL.

In addition to usage, loading characteristics and physical properties of the material play a role in how quickly degradation occurs.

Hence, metrics relating to material degradation are good indicators of End-of-Life (EOL). To measure the suitability of a degradation metric for a physics-based approach to RUL, it is expected to:

- Be physically meaningful values: the metric must be explainable from a physical perspective. For example, the spring constantly defines the stiffness of the spring or the internal resistance of the battery.
- Calculatable from physical measurements: degradation metrics must be available from live measurements from the system, directly or indirectly
- Time varying: for the RUL to be predictable, the metric is expected to trend proportional to the usage and wear of the material, thus changes over time
- Inputs into the state space equation: not only do the degradation metrics need to be derived from the measured variables, but they must be vital to forming the state space equations, thus directly being linked to the system dynamics
- Change in metric leads to change in measurable system behavior: completing the loop, metric changes lead to changes in the system dynamics, measurable in the state variables

Material property-based degradation metrics may be found in components and parts:

| Example | Degradation Metric | Sensor Measurements |
|---|---|---|
| Fan blades of a Turbo Fan | Elastic Modulus | Intake flowrate, strain (in blades) |
| Piping | Elastic Modulus | Pressure, strain gauge |
| Springs | Spring Constant | Displacement, Force |

**Table 1: Examples of degradation metrics related to stress and strain**

However, there are such degradation metrics besides those linked to stress or strain of the material in table 2.

| Example | Sensor Measurements |
|---|---|
| Carbon fiber | Electrical conduction |
| Thermal materials | Thermal conduction |
| Batteries | Current, internal resistance |

**Table 2: Examples of indirect degradation metrics**

## 3. INTERDEPENDENCIES IN DEGRADATION METRICS

While estimating the Remaining Useful Life (RUL) of systems with multiple degrading components is a standard capability of Reliability-Centered Maintenance (RCM) tools used across industry, these methods frequently lack the granularity to rank the most impactful contributors to overall system degradation or to capture the interdependencies through which one component's deterioration may accelerate the degradation of another. This shortcoming can result in interdependence between the degradation metrics, which can potentially contribute to underestimating time to failure (Liao, Peng, Xu, Gui, Yang, Yang & Gui, 2024), reducing maintenance effectiveness, or in the worst case not being able to prevent a predictable failure event.

This is different than multi-modal failures, where there the patterns for multiple failure modes require handling when predicting the degradation metric – for the purpose of the method discussed in the paper, a single failure mode is considered, with interdependencies in the degradation metrics. RUL involving multiple failure modes for the same component would be handled similarly to loading characteristics – expand the historical data, when available to include examples of metrics with multiple failure modes.

Such dependencies are often circular, leading to a positive feedback loop when degradation occurs, such as in the case of batteries where higher internal resistance leads to more heat, more heat leads to higher internal resistance; this would further strain the cooling system, causing more interdependencies. The complex link between interconnected degradation metrics makes it difficult to establish a mathematical model to describe their relations. Therefore, a data-driven method is chosen to build those links empirically via historical operational data, limited run-to-failure data of similar components/parts (Li, Zheng, Xiang, Liu & Wan, 2025).

Interdependencies are often left out of the prediction workflow because data relating to connections between degradation metrics is not available. This may be due to poor collection practices (such as lack of sensor placement) or bureaucratic reasons (such as only providing access to the suspected leading contributor component, the degradation metric for which is interdependent with others). While the techniques explored in this paper do not attempt to detect interdependence, there may be methods in using Digital Risk Twins (Zaman, Z., Apostolou, E., Stecki, C., 2022) to extract information about relationships between components, hence possibly determining the same about degradation metrics.

## 4. PROPOSED SOLUTION

The method discussed in the paper is to handle prediction of RUL in a system with interdependent degradation metrics. To this end, certain pre-requirements are assumed:

- The physics of the system/component, i.e. the system of state space equations is known
- Chosen degradation metrics follow the rules stated earlier and are derived from state variables, and are involved in the system of state space equations
- Historical run-to-failure data is available (without this, either the forecasting must be informed from user-defined interdependency mapping or interdependence is ignored and component-based RUL is used)
- Measured values correspond to state variables

### 4.1. Workflow in detail

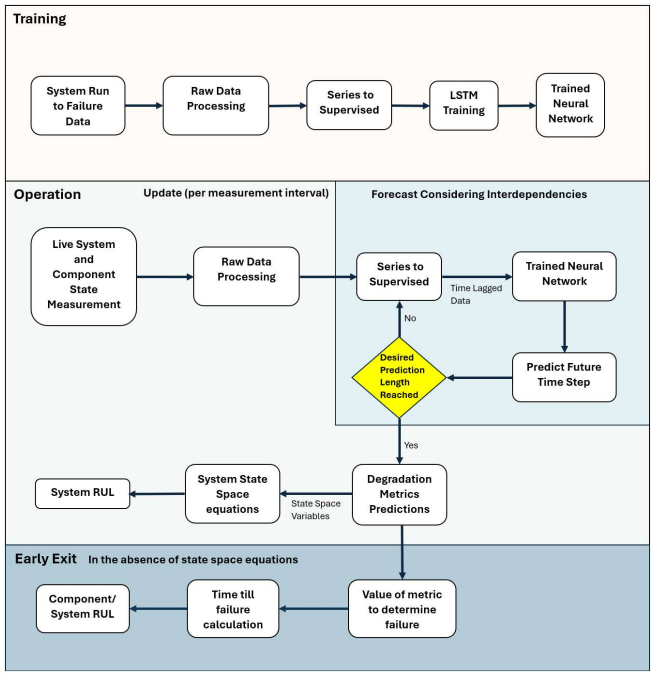


**Figure 1: Proposed solution workflow**

While this is a predominantly physics-based approach, due to the difficulty in modelling interdependence, use of correlation tools will be involved. In the case where interdependencies are not present or a single degradation metric is used, forecasting could be accomplished using a curve-fit on data or using a known curve for the expected trend (would not require data)

The methodology is as follows:

- The degradation metric forecasting method is to be trained using run-to-failure data.
  - The degradation metric is calculated off measured state variables
  - It is rearranged/embedded to represent a set of present-to-future labelled data
  - Train a neural network involving Long-Short Term Memory (LSTM, a method to handle long term forecasting and regression tasks) (Vennerød, Kjærran and Bugge, 2021) cells to learn and predict future degradation metric values taking their interdependence into account
- During operation, the degradation metrics are calculated from the live, measured state variables
  - The forecasting method is fed in some amount of data, which is then used to generate future values
  - These values are then fed back into the forecaster to predict further
  - This cycle is repeated up to a set time forward (horizon)
  - The forecasted results are fit onto a curve to derive an analytical expression to be used as a time-dependent variable in the state space equations for the system
  - The differential equations (from the state space representation) are then solved to obtain an expression for the system variable
  - Using the forecasts obtained, the user can then determine at what values a failure may occur and hence calculate RUL
- In the case where the user has knowledge of a value for the degradation metric(s) that indicates a failure, they may bypass solving the state space equations and using the forecasted degradation metric values directly to derive RUL

### 4.2. Case where run-to-failure data is not available

Collecting run-to-failure data is often difficult, especially in mission-critical systems or components, where failure is expected to be rare. In such cases, a neural network or any method requiring historical data is not possible. Occasionally, the user of the system may know, from usage, experimentation or otherwise, a custom expression to define the degradation metrics as a function of time. If this is not available, then the only option is to pursue a component-based RUL using an estimated curve to fit and forecast the degradation metrics and risk underestimation of the RUL prediction.

## 5. CASE STUDY

A case study was conducted to demonstrate an application of this method. An aircraft landing gear system experiencing cyclic loading from multiple landing cycles was selected as a multi-component system without needing an overly complex

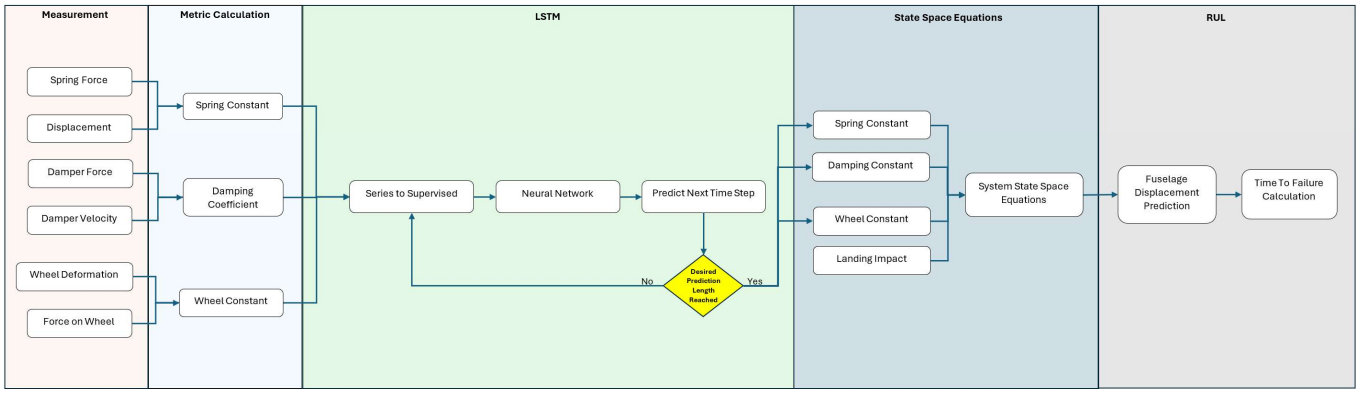


**Figure 2: Detailed workflow of aircraft suspension RUL**

mathematical model. In the absence of access to experimental data the system behavior was mathematically simulated in MATLAB instead. Figure 2 provides an entire start-to-finish workflow for this case study.

### 5.1. System Definition

The aircraft undercarriage was modelled off an Airbus A320. This aircraft's landing gear are in a tricycle arrangement with two main landing struts located near the center of its mass and one nose landing gear. The main landing struts were considered to bear all the force in the initial landing impact with no force being distributed to the nose gear within the chosen window length. Hence the strut was modelled as one main landing gear experiencing the load from half the aircraft during landing with the aim of using measurements of the wheel deformation ($z_W$), suspension deformation ($z_S$), velocity of oscillation (v), force upon the wheel ($F_W$), force upon the damper ($F_D$) and force upon the suspension spring ($F_S$) in conjunction with a neural network and system state equations to determine the RUL of the landing strut.

The suspension spring, damper and tire stiffness were chosen as the three simultaneously degrading components that would ultimately lead to system failure.

Catastrophic system failure was deemed to be when the suspension exceeded the safe maximum stroke (approx. 0.5m) which roughly corresponded to when engine pod strike would occur.

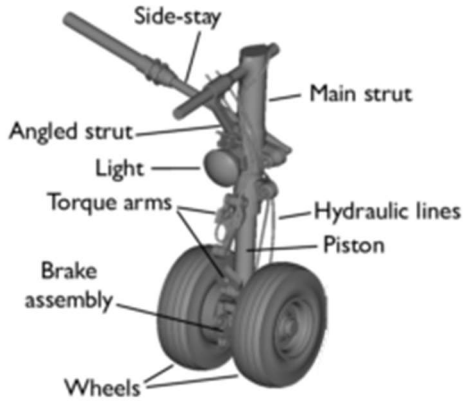


**Figure 3: Diagram of aircraft strut (Xia, 2025)**

The system shown in figure 3 was decomposed into the physical system shown in figure 4.

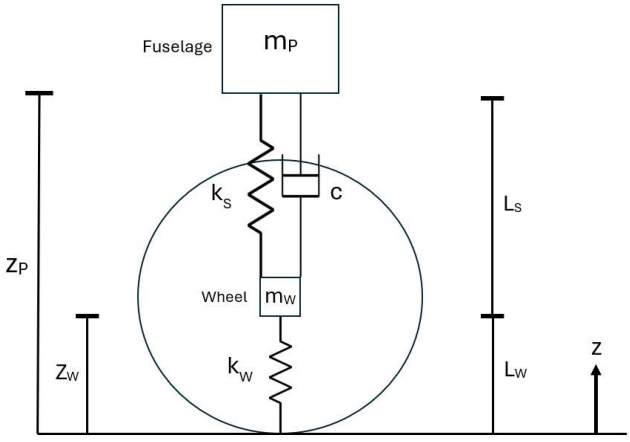


**Figure 4: Simplified physics model of the aircraft strut**

Although aircraft landing gear in commercial airliners such as the Airbus A320 typically use OLEO struts, a simplified spring damper system was proposed to simplify the model as OLEO struts exhibit nonlinear behavior when under compression which would introduce unnecessary

complexity. The tire of the wheel was modelled as a spring connecting the runway to the point mass positioned at the center of the wheel. All motion will be assumed to be in the vertical plane. Upwards displacement was taken to be positive.

Using newtons second law (F = ma) equations of motion were derived for the system described in figure 4.

$$\sum F_P = m_P \ddot{z_P} \tag{1}$$

$$\sum F_W = m_W \ddot{z_W} \tag{2}$$

$$m_P \ddot{z_P} = -k_s((z_P - z_w) - L_S) - c(\dot{z_P} - \dot{z_w}) - m_P g \tag{3}$$

$$m_w \ddot{z_W} = k_s((z_P - z_w) - L_S) + c(\dot{z_P} - \dot{z_w}) - k_w(L_W - z_w)^+ - m_w g \tag{4}$$

The positive part function works as defined in equations 5.

$$x^+ = \max(x, 0) \tag{5}$$

Equation 5 is necessary to correctly model the interaction between the runway and tire as it accounts for the fact that the wheel cannot experience tensile force.

Equations 3 and 4 were then transformed into state space form using the following vector transformation.

$$\begin{bmatrix} z_C \\ \dot{z_C} \\ \ddot{z_C} \\ z_W \\ \dot{z_W} \\ \ddot{z_W} \end{bmatrix} \rightarrow \begin{bmatrix} Z_1 \\ Z_2 \\ Z_3 \\ Z_4 \end{bmatrix} \tag{6}$$

Where:

$$z_C = Z_1 \tag{7}$$
$$\dot{z_C} = Z_2 \tag{8}$$
$$z_W = Z_3 \tag{9}$$
$$\dot{z_W} = Z_4 \tag{10}$$

The final system state space equations become:

$$\dot{Z_1} = Z_2 \tag{11}$$
$$\dot{Z_3} = Z_4 \tag{12}$$
$$\dot{Z_2} = \frac{-k_s}{m_P}((Z_1 - Z_3) - L_S) - \frac{c}{m_P}(Z_2 - Z_4) - g \tag{13}$$
$$\dot{Z_4} = \frac{k_s}{m_W}((Z_1 - Z_3) - L_S) + \frac{c}{m_W}(Z_2 - Z_4) - \frac{k_w}{m_W}(L_W - Z_3)^+ - g \tag{14}$$

The degradation metrics chosen to represent the health of the system were: suspension spring constant ($k_S$), damping coefficient (c) and wheel stiffness ($k_W$).

These metrics satisfy the previously discussed conditions for valid degradation metric selection as they:

- Describe the physical properties of the materials.
- Can be computed from physical measurements.
- Given the long lifespan of aircraft landing gear can be considered as time varying.
- Are terms within the system equations.
- Changes in their values directly impact system behavior.

### 5.2. Data Simulation

A simulation of the system dynamics was constructed in order to generate both training and operational data. This section documents the process taken in defining system constants and conditions, modelling degradation and finally simulating the system response to generate measurement data.

#### 5.2.1. Assumptions

Throughout the process it was assumed that:

- Velocity of the wheel relative to the fuselage was 0m/s before landing impact.
- The landing gear was stretched to a static equilibrium displacement due to gravity acting on the wheel just before landing.
- No reaction force is experienced by the landing strut from the ground at t=0s.
- The simulation began at the same time as landing impact.
- Main landing gear suspension components will obey Hooke's Law and the Viscous Damping Law.
- Load is evenly distributed between the two landing gear (no roll).

#### 5.2.2. Aircraft Dimensions

All dimensions and specifications are modelled off an Airbus A320.

**Initial Wheel Stiffness**

An Airbus A320 typically uses a 46x17R20 tire size (Rotable Repairs Ltd, 2025). A typical tire pressure of 210psi is used as specified by Airbus's 'Aircraft Characteristics Airport and Maintenance Planning', 2023.

Although tire stiffness follows non-linear behavior for the sake of simplicity it was assumed to obey Hooke's Law. Using the above specifications and equations 15-17 an approximate tire stiffness was computed.

$$A = \frac{m_P g}{2P} \tag{15}$$

$$V = \pi(R^2 - r^2)w \tag{16}$$

$$k_{W0} = 2\gamma \frac{PA^2}{V} \quad (17)$$

Equation 20 offers an approximate contact area of the tire at rest ignoring side wall deformation. Note: only a quarter of the planes total weight is used as the load as there are two tires per strut.

Equation 21 offers an approximate formula for the internal volume of the tire, where R and r are the outer and inner radii of the tire respectively and w is the width.

Finally, equation 22 provides an estimate of the combined initial spring constant for both wheels of the landing strut acting in parallel. Compression is assumed to be isothermal due to the fact the wheel is at equilibrium for a long period of time, hence $\gamma = 1$ is assumed.

**Initial Suspension Spring Stiffness**

Initial suspension stiffness was calculated using the static deflection value (approx. 0.15m) for an Airbus A320 and Hooke's Law as shown in equations 18-20.

$$z_{spring\ compression} = z_{aircraft\ deflection} - z_{wheel\ compression} \quad (18)$$

$$z_{wheel\ compression} = \frac{k_{W0}}{m_P g} \quad (19)$$

$$k_{S0} = \frac{m_P g}{z_{spring\ compression}} \quad (20)$$

**Relaxed Spring Length**

As shown in equation 21 relaxed length of the suspension spring was finally computed according to the static equilibrium position of the Airbus A320's fuselage position above the runway (approx. 1.75m).

$$L_S = h + z_{total\ aircraft\ deflection} - R \quad (21)$$

Where h is the height of the fuselage above the ground and R is the relaxed outer radius of the wheel.

**Initial Damping Coefficient**

A damping coefficient of $c = 87000Ns/m$ was proposed by (Shi, Cai and Wang, 2020) to be an appropriate value for modelling an oil damped commercial aircraft strut.

A summary of all the calculated aircraft dimensions computed using equations 20-26 is presented in table 5.

| Constant | Value |
|---|---|
| $k_{W0}$ | $4.6MN/m$ |
| $k_{S0}$ | $2.4MN/m$ |
| $L_W$ | $0.58m$ |
| $L_S$ | 1.32m |
| $c$ | $8.7kNs/m$ |

**Table 5: Summary of dimensions and values for A320 landing strut.**

Other keys dimensions are listed in table 6:

| Constant | Value |
|---|---|
| $m_P$ (half max landing weight) | $32500kg$ |
| $m_W$ | 120kg |

**Table 6: Values of other important system constants**

**5.2.3. Initial Conditions**

- The initial position of the wheel was computed according to equation 22:

  $$y_{W0} = L_W \quad (22)$$

- The initial position of the fuselage was computed using equation 23:

  $$y_{P0} = L_S + L_W + \frac{mg}{k_W} \quad (23)$$

  Where the third term on the right hand side represents the displacement of the wheel from its relaxed position due to the suspension spring being stretched by the gravitational force on the wheel.

- The velocity of the wheel and fuselage relative to one another was assumed to be 0m/s, thus $v_{P0} = v_{W0}$.

  The sink rate of the plane at landing was modelled as a lognormal distribution with a mean of -0.6m/s truncated between -0.4m/s and -1.2m/s. This model offered a realistic variation of landing impact whilst maintaining safe landing conditions for an A320 as outlined by Airbus.

  Equation 24 presents the form of the lognormal distribution before truncation.

  $$v_{S0} = v_{W0} = \frac{-1}{x\sigma\sqrt{2\pi}} e^{-\frac{1}{2}\left(\frac{\ln x - \mu}{\sigma}\right)^2} \quad (24)$$

  Where: $\sigma = 0.4$ and $\ln 0.6$

**5.2.4. Degradation Modelling**

In the absence of experimental degradation data a novel mathematical model of material and component degradation was proposed. The formulation of this model is detailed within this section.

The damper was modelled to degrade independently of other system components. Both the wheel stiffness and suspension spring were modelled to degrade in response to the failing damper as suggested by TSHGS, 2023 'if another suspension component fails, causing a cascading effect that damages the spring'.

Equations 25-29 provide an example of this proposed modelling.

Equation 25 represents the form of the equation used to model the damper health degradation.

$$H_c^i = a_1^i + a_2^i \exp\left(-a_3^i N^{a_4^i}\right) \quad (25)$$

Equations 26 represents the form of the equation used to model wheel and spring health degradation.

$$H_k^i = a_5^i + \frac{a_6^i}{1+\exp\left(k_{vals}^i (N - N_0^i)\right)} \quad (26)$$

Degrading functions for the three degradation metrics were then generated using equations 27-29.

$$c = c_0 H_c^i \quad (27)$$

$$k_s = k_{s0}(0.5 + 0.5H_k^i) \quad (28)$$

$$k_w = k_{w0}(0.7 + 0.3H_k^i) \quad (29)$$

5 variations of the previously defined degradation functions were generated using the constants shown in table 7.

| | |
|---|---|
| $a_1^i$ | $[0, 0, 0, 0, 0.05]$ |
| $a_2^i$ | $[1, 1, 1, 1, 0.95]$ |
| $a_3^i$ | $[0.0075, 0.006, 0.0055, 0.0065, 0.006]$ |
| $a_4^i$ | $[1, 1, 1, 1.3, 1]$ |
| $a_5^i$ | $[0, 0, 0, 0, 0.05]$ |
| $a_6^i$ | $[1, 1, 1, 1, 0.95]$ |
| $k_{vals}^i$ | [0.05, 0.04, 0.035, 0.045, 0.038] |
| $N_0^i$ | [215, 225, 230, 220, 235] |

**Table 7: Constants for 5 varied degradation models.**

The constants chosen above are somewhat arbitrary and predominantly focus on providing interdependent modelling of degradation for the neural network to learn from. Accurate mathematical modelling of material fatigue is difficult without access to specific experimental data.

### 5.2.5. Simulation

Equations 11-14 were solved using the conditions, values and models presented in sections 5.2.1-5.2.4. The simulation was run 5 times in order to produce enough data to effectively train, validate and test the neural network.

- For each of the 5 data sets the system of ODEs were solved 400 times with each iteration spanning a 10s window after the landing impact.
- Each iteration, N was incremented by 1 to compute the next cycle's degradation metrics values.
- The solutions to the ODEs returned the values of $y_P$, $\dot{y}_P$, $y_W$ $and$ $\dot{y_W}$.
- The force upon the spring, damper and wheel along with the component deformation and velocity were then computed using Hooke's Law and the Viscous Damping Law.
- The final data sets were each of size 40000x7, where each column corresponds to system measurements of: Time, deformation of the spring, velocity of the damper, deformation of the wheel, force on the spring, force on the damper and force on the wheel, and each row represented one landing cycle.

Figure 5 provides an example of one of the variations of the degradation modelling.

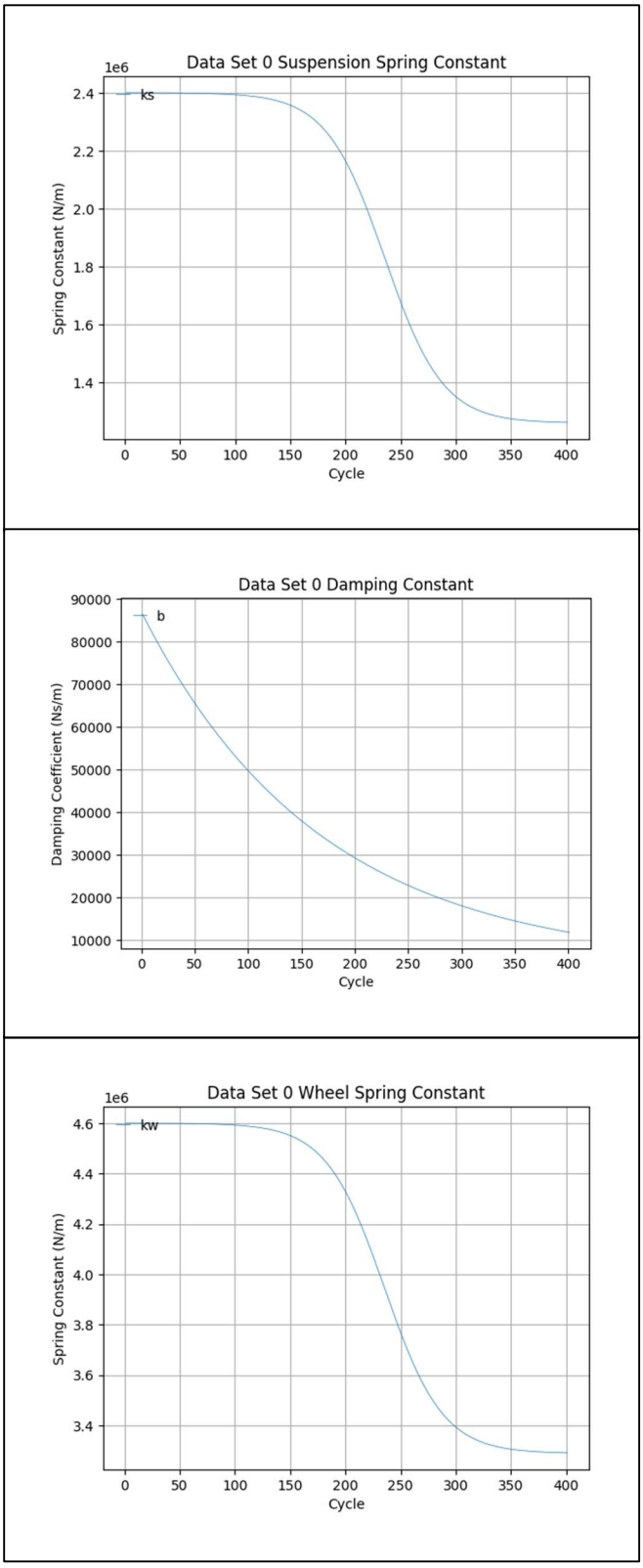


**Figure 5: Example of interdependent degradation functions**

Figure 6 shows the fuselage's and center of the wheel's position relative to the runway after landing under the influence of a healthy landing gear system.

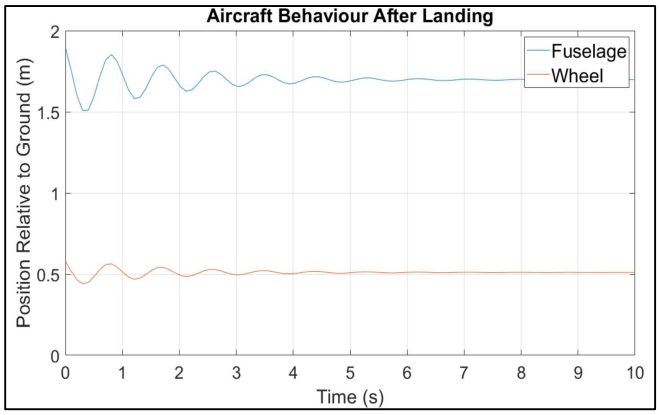


**Figure 6: Position of wheel and fuselage relative to runway after initial landing impact.**

### 5.3. Results

#### 5.3.1. Neural network forecaster prediction

All 5 data sets underwent preprocessing where the average suspension spring constant, damping coefficient and wheel spring constant were computed for each landing cycle according to Hooke's Law and the Viscous Damping Law. This raw data processing returned data sets similar to those shown in figure 5.

A scaler was fitted to all data before then being used to scale 4 of the data sets individually. The scaler had to be fitted to all data in order to preserve the correct relative size of data across sets. The scaler scaled all data between 0 and 1.

3 sets were used for the forecaster training where they were individually put into a supervised format before being vertically stacked and shuffled for best model generalization. 1 set, also in a supervised format was used as validation data. A summary of the neural network architecture is provided in figure 6. An overview of the neural network hyperparameters is presented in table 7.

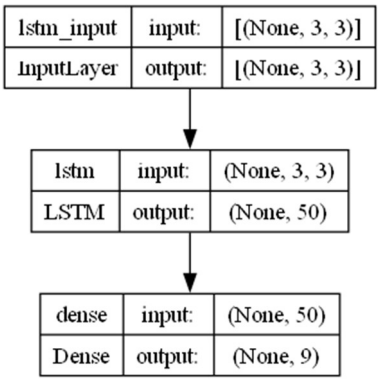


**Figure 6: Neural network architecture**

| Hyperparameter | Value |
|---|---|
| Epochs | 25 |
| Batch size | 65 |

**Table 7: Neural Network Hyperparameters**

The final set was used as test data. The test data represents in operation data that is being gathered live every landing cycle.

The first 50% (200 cycles) of the test data set is fed into the neural network to represent the 200 landings the aircraft suspension has currently been through. The aim is to then predict the degradation trends over 200 future landing cycles.

The forecaster recursively makes predictions until the full 400 cycle range is filled as shown in the 'LSTM' section of the workflow in figure 2.

The resulting prediction shown in figure 7 compares the quality of the predictions to the true future system behavior.

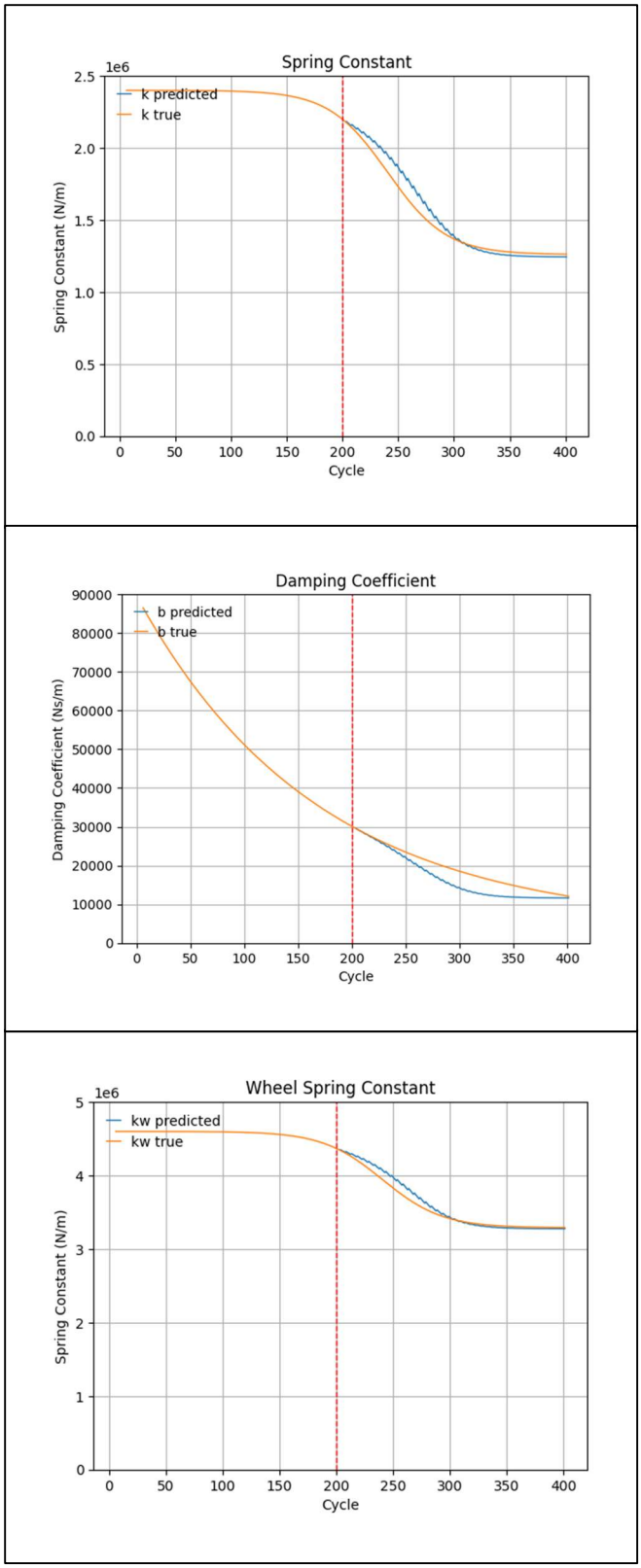


**Figure 7: Degradation metric predictions vs measured values**

Note: The dotted line represents the measurement horizon; hence, the neural network is making predictions based only on the data prior to the horizon. After the horizon is the comparison between predictions and measured system behavior as per the simulation results.

### 5.3.2. State Space Prediction

The degradation metric forecast combined with the system state space equations 11-14 were used to compute the behavior of the suspension system per forecasted cycle. The initial conditions were computed as shown in section 5.2.3 with the sink rate continuing to be modelled as a truncated lognormal distribution.

As shown in figure 8 when the landing gear is healthy suspension stroke decays quickly and does not exceed amplitudes which cause damage to the aircraft.

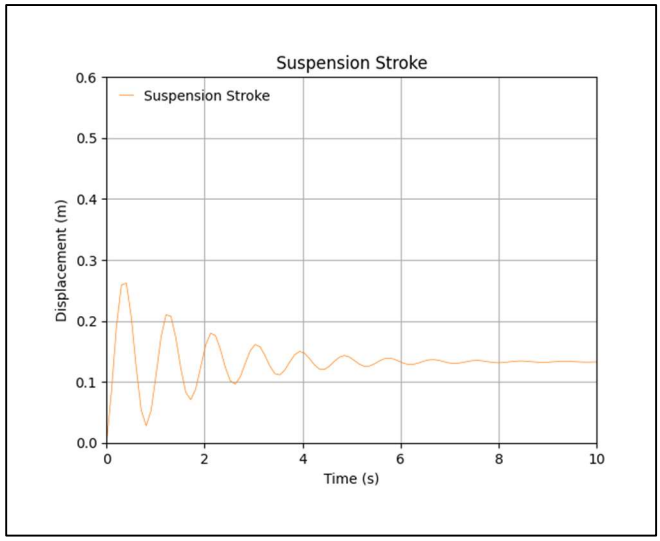


**Figure 8: Healthy landing response on 1st cycle.**

Note: Positive stroke values correspond to spring compression.

Each cycle the model checks if the previously defined failure mode has occurred (suspension stroke exceeding maximum safe stroke). In the case where failure is detected in the predicted behavior the current cycle under analysis is returned as the system RUL.

Equation 30 shows how suspension stroke and failure is calculated.

$$L_S - (y_P - y_W) > 0.5m \tag{30}$$

Figure 9 shows a comparison between the system behavior at the predicted cycle of failure and true system behavior at the cycle when the system failed.

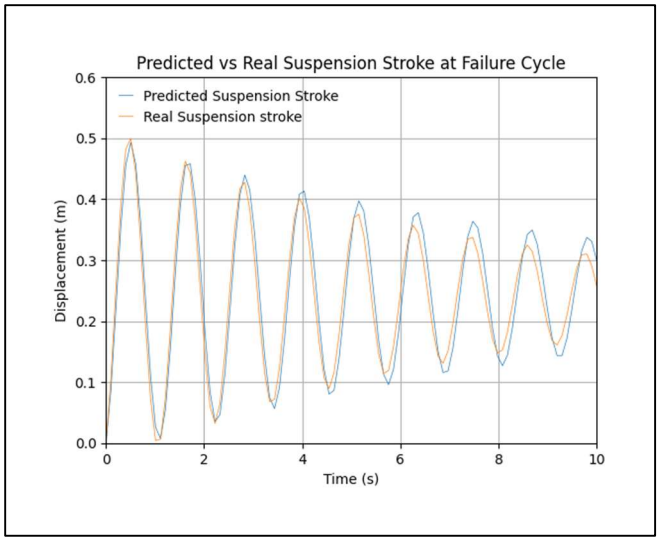


**Figure 9: System behavior at time of failure.**

The model predicted failure would occur on the 306th cycle and real failure occurred in the simulation on the 305th cycle. As can be seen in figure 9 the system behavior at the real and predicted failure cycles is near identical and the only discrepancy arises from the difference in the cycle in which failure occurred. Ultimately the model was able to predict failure within 1 cycle of true system failure 105 landing cycles in advance.

### 5.4. Increasing Complexity

In addition to the current model, there is capacity to include greater variation and inconsistencies in landing descent speed (including landings classified as 'hard') and landing acceleration with the requirement that the training data includes these variations in order for the neural network to learn the degradation patterns.

## 6. IMPLEMENTATION INTO A MAINTENANCE PROCESS

Maintenance is the driving use-case for RUL predictions, since scheduling and planning revolves around when the machine is expected to fail. A theoretical plan to implement the process described thus far would similarly to sections 4 and after in Mitici, Pater, Barros and Zeng, 2023. Firstly, it is assumed that the machine is in its design stage, allowing for better data collection from tests as well as samples collected from similar assets' run-to-failure/EOL data. Since this is expected to run with the system operating live, the maintenance scheduling is to happen over a period (horizon) of events forecasted into the future. Staff would mainly involve engineers or maintenance supervisors planning using the predicted values when a failure is expected to occur.

Multiple components need to be handled when failure is predicted – this could be handled with separate failure detection and isolation tools once the future system state is

predicted to isolate the specific failure. Once the 'root' component/part is located, maintenance can be scheduled for those areas.

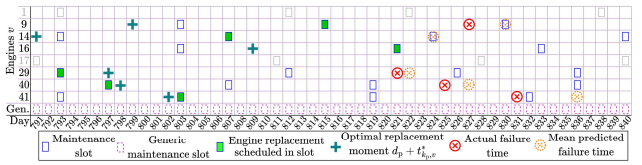


(a) Present day $d_p = 791$. Not depicted is that engine 14 fails at day 843, and that engine 16 fails at day 854, while the mean predicted failure time is at day 845.

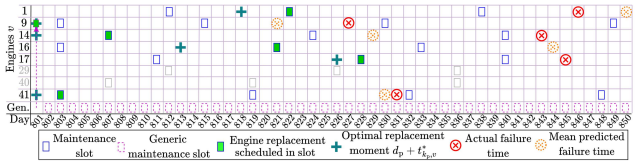


(b) Present day $d_p = 801$. Not depicted is that engine 16 fails at day 854, and that the mean predicted failure time of engine 17 is at day 852.

**Figure 10: Excerpt from Mitici et al, showcasing the maintenance scheduling procedure of systems**

In figure 3, a similar maintenance methodology is expressed in Mitici et al (albeit using a more correlation-based approach for the RUL prediction).

## 7. CONCLUSION

Remaining useful life prediction using the physics of the system is understated, often overshadowed by correlation tools. While these are sometimes used in conjunction with subject matter (SME) experts to build hybrid solutions for forecasting, however the metrics chosen to represent degradation make for a guess at indicating system health. The method presented in this paper outlines a physics-based approach with a focus on using material properties (which show clear signs of change for wear and fatigue), along with knowledge of system dynamics to predict RUL. To that end, a suspension system was used to demonstrate the applicability of the method proposed, using simulated data. Expanding upon this work, the aim is to include the effect of shocks, loading characteristics and further case studies with different systems.

## NOMENCLATURE

| | |
|---|---|
| $t$ | Time (s) |
| N | Cycle |
| $m_P$ | Mass of half plane (kg) |
| $m_W$ | Mass of wheel (kg) |
| $y_P$ | Displacement of fuselage (m) |
| $\dot{y}_P$ | Velocity of fuselage (m/s) |
| $\ddot{y}_P$ | Acceleration of fuselage (m/s^2) |
| $y_{P0}$ | Initial fuselage position (m) |
| $y_W$ | Displacement of COM of wheel (m) |
| $\dot{y}_W$ | Velocity of COM of wheel (m/s) |
| $\ddot{y}_W$ | Acceleration of COM of wheel (m/s^2) |
| $y_{W0}$ | Initial wheel position (m) |
| $F_P$ | Force on the fuselage (N) |
| $F_S$ | Force on the spring (N) |
| $F_D$ | Force on the damper (N) |
| $F_W$ | Force on the wheel (N) |
| $k_W$ | Wheel spring constant (N/m) |
| $k_{W0}$ | Initial wheel spring constant (N/m) |
| $k_S$ | Initial suspension spring constant (N/m) |
| $k_{S0}$ | Suspension spring constant (N/m) |
| $b$ | Damping Coefficient (Ns/m) |
| $b_0$ | Initial damping Coefficient (Ns/m) |
| $v_{P0}$ | Initial fuselage velocity (m/s) |
| $v_{W0}$ | Initial wheel velocity (m/s) |
| $L_S$ | Relaxed length of suspension spring (m) |
| $L_W$ | Relaxed length of wheel (m) |
| A | Static contact area of the tire (m^2) |
| P | Internal tire pressure (Pa) |
| V | Internal volume of the tire (m^3) |
| $\gamma$ | Heat capacity ratio |
| $g$ | Acceleration due to gravity (m/s^2) |

## REFERENCES


Beaulieu M. H. & Jha M. S. & Garnier H. & Cerbah F., (2024). Remaining Useful Life prediction based on physics-informed data augmentation. *Reliability Engineering & System Safety* (Volume 252), doi:10.1016/2024.110451

Wang Y., Zhao Y., & Addepalli S., (2020). Remaining Useful Life Prediction using Deep Learning Approaches: A Review, *Procedia Manufacturing*. (Volume 49, Pages 81-88), doi:10.1016/2020.06.015

Liao J., Peng T., Xu Y., Gui G., Yang C., Yang C., Gui W., (2024). Task-orientated probabilistic damage model with interdependent degradation behaviors for RUL prediction of traction converter systems, *Reliability Engineering & System Safety*. (Volume 250), doi:10.1016/2024.110302

Li Z., Zheng H., Xiang X., Liu S., Wan Y., (2025). Remaining useful life prediction with limited run-to-failure data: A Bayesian ensemble approach combining mode-dependent RVM and similarity, *ISA Transactions.* (Volume 156, Pages 307-319), doi:10.1016/2024.11.023

Vennerød C. B., Kjærran A. and Bugge E. S., (2021). Long Short-term Memory RNN, *arXiv,* doi: 2105.06756

Mitici M., Pater I. d., Barros A., Zeng Z., (2023). Dynamic predictive maintenance for multiple components using data-driven probabilistic RUL prognostics: The case of turbofan engines, *Reliability Engineering & System Safety*, doi: 10.1016/2023.109199

Ott, L., Gräber, T., Unterreiner, M., Edelmann, J., Plöchl, M., (2024). Simulating Effects of Suspension Damper Degradation on Common Sensor Signals for Diagnosis Models in the Context of Condition-Based Maintenance. In: Mastinu, G., Braghin, F., Cheli, F., Corno, M., Savaresi, S.M. (eds) 16th International

Symposium on Advanced Vehicle Control. AVEC 2024. Lecture Notes in Mechanical Engineering. Springer, Cham. https://doi.org/10.1007/978-3-031-70392-8_122

TSHGS. (2023) *How Long Do Coil Springs Last*. Available at: https://www.tshgcoilspring.com/resources/how-long-do-suspension-springs-last.html (Accessed: 27 May 2025).

Xia S. (2025) Why Is CNC Machining the Future of Aircraft Landing Gear Systems?. Available at: https://bccncmilling.com/why-is-cnc-machining-the-future-of-aircraft-landing-gear-systems/ (Accessed: 27 May 2025).

Zaman, Z., Apostolou, E. & Stecki, C. (2022) Predictive Maintenance for Safety-critical systems with a Digital Diagnostic Twin, *International Conference on System Safety.*

Rotable Repairs Ltd. (2025) *Airbus A320.* Available at: https://rotablerepairs.com/a320-airbus.html (Accessed: 9 May 2025).

Xingang S., Liangcai C., Guanhu W. & Lei L. (2020) A New Aircraft Taxiing Model Based on Filtering White Noise Method, *IEEE Access, Volume 8*. doi: 10.1109/ACCESS.2020.2964754, IEEE

Bardou N. & Owens D. (2014) Hard Landing, a Case Study for Crews and Maintenance Personnel, *Safety First, Issue 17.*

Airbus (2023). A320, AIRCRAFT CHARACTERISTICS AIRPORT AND MAINTENANCE PLANNING, AC. *AIRBUS S.A.S. Customer Services, Technical Data Support and Services, 31707 Blagnac Cedex, FRANCE*

## BIOGRAPHIES

**Navid T. Zaman** is the Lead Data Scientist at PHM Technology, mainly working on causation-based AI and failure detection and isolation tool Syndrome Diagnostics. His main responsibilities are around R&D involving data-driven and AI technologies.

**Milo S. Cooper** is a current student at the University of Melbourne studying mechatronics engineering. His interests align mainly with the research of engineering reliability solutions.

**Frank M. Juarez** has worked in the defense aerospace industry since 2004, mainly supporting depot, RCM, and CBM programs. He currently serves as Vice President of Engineering over U.S. Operations for PHM Technology. Previously, he was Chief Reliability Engineer & Manager at Redhorse Corporation, overseeing reliability engineering for the USAF and USMC CBM+ programs. From 2009 to 2022, he served as a Senior Reliability Engineer at StandardAero, supporting USAF RCM and NAVAIR engine depot programs. Frank attended the University of Texas at San Antonio and Embry-Riddle Aeronautical University, is an active member of the SAE Integrated Vehicle Health Management aerospace standards committee as well as the RAMS working groups facilitated by the Office of the Under Secretary of Defense for Research & Engineering, Systems Engineering & Architecture. He has a passion for experimental homebuilt aircraft and resides near San Antonio, Texas.